JOURNAL OF GUIDANCE, CONTROL, AND DYNAMICS
Vol. 21, No. 1, January–February 1998

Vision-Based Position and Attitude Determination for Aircraft Night Landing

Gano B. Chatterji*
Sterling Software, Moffett Field, California 94035
Padmanabhan K. Menon†
Optimal Synthesis, Palo Alto, California 94306
and
Banavar Sridhar‡
NASA Ames Research Center, Moffett Field, California 94035

An image-based method for the determination of aircraft position and yaw and pitch orientations with respect to the runway during night landing is described. Information derived from a model of the airport lights together with video images acquired by an onboard video camera and roll attitude angle sensed with a roll sensor are integrated in a Kalman filtering algorithm. Simulation results are presented to demonstrate the feasibility of the proposed concept.

I. Introduction

LANDING is one of the most demanding flight regimes in fixed-wing aircraft operations. It involves controlling and coordinating all six degrees of freedom of the aircraft to bring it in coincidence with a reference path to the touchdown point on the runway. Due to the complexity of the task, landing phase of flight alone accounts for 29% of the accidents. Approach and landing accidents together account for 41% of the accidents.[1] Additionally, research shows that night approach accident rates are about eight times the day rate.[2] This is attributable to difficulties associated with reduced lighting during the nighttime hours. For example, cockpit references, ground references, navigation, landings, and the abilities to gauge the position and speed of other air traffic are significantly impacted during periods of darkness. Furthermore, the human body is primarily adapted for daytime activity. Night flying places the pilot's eyes, which provide the primary sensory information needed for flight, in an environment for which they are only partially suited. Limitations of the human visual system along with aircraft motion are responsible for numerous static and dynamic illusions that have dangerous implications during night landing.[3] Thus, in addition to the usual landing hazards such as windshear and crosswind, and difficulties such as complex approach procedures employed at airports near population centers, night landing can further add to the pilot workload.

The chief motivation for the current research is to produce a pilot aid that can help reduce night approach and landing accidents. Although cockpit instruments allow the pilot to determine the orientation with respect to the local horizontal and position with respect to some reference location such as the departing airport, they do not directly provide position and attitude of the aircraft relative to the runway desired for landing. Landing aids such as the Instrument Landing System (ILS) and the Microwave Landing System (MLS) can be used to ameliorate the difficulties. However, due to their cost, these systems are likely to be available only at a few major airports. Emerging Global Positioning System (GPS) technologies can also be used for this purpose. In the future, systems such as integrated Inertial Navigation System/Differential GPS are expected to deliver the accuracies needed for landing.[4] Given the advantages of all-weather landing at any airport, large commercial air carriers may equip their airplanes with such systems. Currently, ILS systems are available at major U.S. airports that are used by these air carriers to land their airplanes. Unlike these large air carriers, air carriers and general aviation aircraft that are not equipped with ILS receivers can use only visual landing aids such as approach and runway lighting to obtain alignment guidance. Glide slope information during visual approach is provided by visual approach slope indicator or precision approach path indicator lights.

The objective of this research is to develop a vision-based system for ILS like pilot aiding for landings at airports without ILS or MLS. A significant advantage of such a system is that instrument approach to most airports will be possible by all classes of aircraft. For ILS or MLS equipped aircraft, such a system could serve as a backup landing system.

There are two possible approaches toward the development of such a system. One is to develop an independent sensor system that accomplishes this goal. The second is to develop a sensor system integrated with a low-cost GPS system such that the combined system generates accurate measurements for landing. In Ref. 5 an integrated GPS–machine vision system for position determination was described. The attitude was assumed to be known. In this paper only the roll attitude information is used. The other two orientations are estimated along with the three components of runway relative position vector. The approach is an extension of the earlier paper. As opposed to the earlier paper, GPS was not used because the purpose here is to explore the limits of a minimally aided vision-based system.

This paper is organized as follows. First the landing operation is described in Sec. II. Next, Sec. III describes the standard airport lighting layout based on Ref. 6. Section IV describes the various reference frames. The vision-based algorithm is described in Sec. V. Details of the simulation and results are given in Sec. VI. The conclusions are summarized in Sec. VII. Finally, implementation details of the Kalman filter are given in the Appendix.

II. Aircraft Landing Operation

The final approach segment of the aircraft arrival flight to the destination airport is used for navigating the aircraft and properly positioning it with respect to the runway to permit safe landing. The procedures commonly used during the final approach are the nonprecision and precision approaches. During precision approach, a precision approach aid is used to fly the aircraft along the final approach path, which is also known as the glide path.[7] Figure 1 shows a 3-deg glide slope approach. Glide slope ν is defined as

$$\tan \nu = h / x_{\mathrm{go}} \tag{1}$$

where h is the altitude and x_{go} is the distance-to-go to the touchdown point. For precision approach, the glide slope is between 2.5

Received Aug. 26, 1996; revision received July 5, 1997; accepted for publication Sept. 3, 1997.

*Member of Professional Staff, MS 262-6. Senior Member AIAA.
†President; also Adjunct Professor, Santa Clara University, Santa Clara, CA 95053. Associate Fellow AIAA.
‡Chief, AFC Branch, MS 262-3. Associate Fellow AIAA.

Table 1 Aviation navigation accuracy requirements

Category	Cross track, ft	Altitude, ft
I	±56.1	±13.45
II	±17.06	±5.58
III	±13.45	±1.97

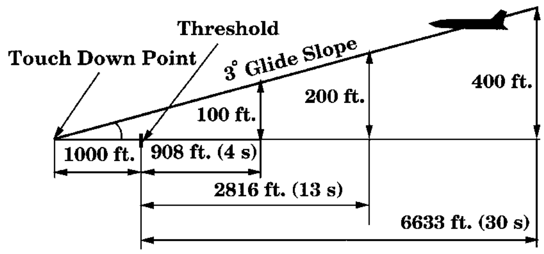

Fig. 1 Glide slope, altitude, time, and distance relationships.

and 3 deg (Ref. 8). The optimum length of the final approach is 5 miles; the maximum length is 10 miles (Ref. 8). The glide slope in conjunction with the location of the touchdown point specifies the desired aircraft position with respect to the runway threshold as a function of altitude. The touchdown point is specified in terms of distance from the runway threshold. From Fig. 1 it may be seen that the 3-deg glide slope requires the aircraft to be at a distance of 6633, 2816, and 908 ft corresponding to altitudes of 400, 200, and 100 ft. These distances translate to 30, 13, and 4 s to the runway threshold for an approach speed of 220 ft/s (130 kn).

Once on the glide slope, the aircraft is flown to a designated altitude known as decision height where a decision must be made by the pilot to continue descent or to abort. There are prescribed landing categories with associated decision heights up to which aircraft can be flown with instruments. Decision heights of 200, 100, and 50 ft correspond to category I (CAT I), II, and III, respectively. The performance specifications for Federal Aviation Administration defined precision approach and landing categories are given in Table 1 (Ref. 9). These accuracy requirements will be used to evaluate the performance of the machine vision-based algorithm described in this paper.

Because the machine vision-based algorithm described in this paper uses information derived from images and the model of the airport lighting layout, the arrangement of airport lights and the information provided by them is discussed in the next section.

III. Airport Lighting Layout

The purpose of airport lighting is to provide information about correct airport/runway identification, approach direction, alignment, and attitude information for safe landing. The lights are placed at fixed distances and color coded to meet these objectives. Standard airport lighting is composed of the approach and runway lights.[6] Both the approach and the runway lighting systems are described next.

Common configurations for approach lighting are the Calvert system and the standard configuration-A system.[6] The Calvert system is widely used in Europe and elsewhere. The standard configuration-A approach lighting system is the national standard for civil and military use in the United States. Both systems are 3000 ft long. Figure 2 illustrates the standard configuration-A approach lighting system.

In the standard configuration-A approach lighting system, the centerline bars are composed of five white lights separated by 40.5 in. There is a sequenced flasher in front of each centerline bar. The distance between the centerline bars is 100 ft. The cross bar, located 1000 ft from the runway threshold, consists of eight white lights on each side of the centerline bar. These lights are separated from each other by 5 ft. The threshold bar is located 10 ft from the runway threshold and consists of green lights arranged 5 ft apart. The threshold bar runs along the entire width of the runway and extends 45 ft beyond the runway on each side. The wing bar is located at a distance of 100 ft from the threshold bar. The wing bar consists of five red lights placed symmetrically about the centerline. The interlight separation is 40.5 in. The terminating bar is located

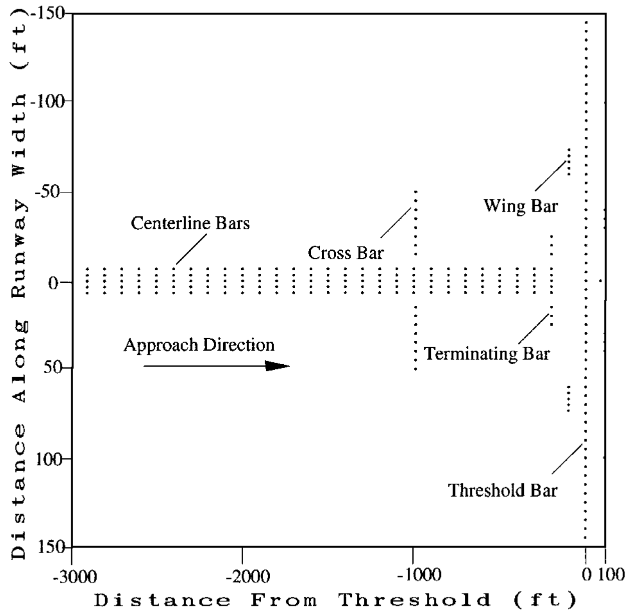

Fig. 2 Standard configuration-A approach lighting system.

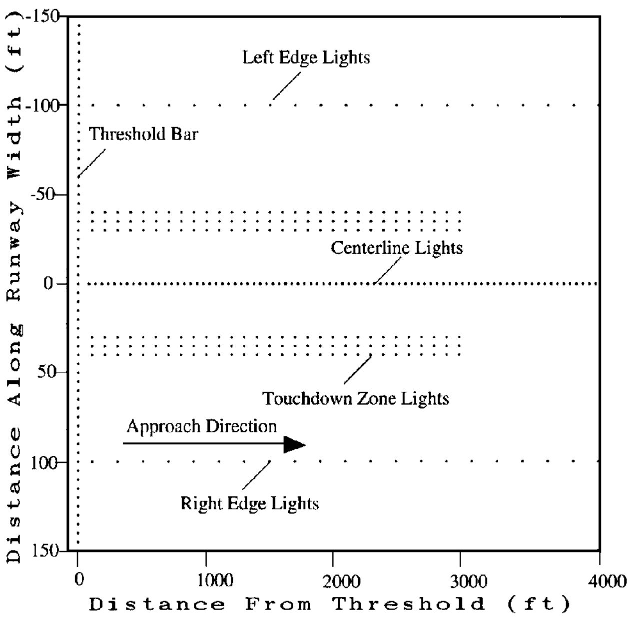

Fig. 3 Runway lighting system.

at a distance of 200 ft from the threshold bar and consists of five red lights, 40.5 in. apart at the centerline, and two sets of three red lights, 5 ft apart, placed symmetrically about the centerline. Approach lights are usually placed on pedestals of different heights. The specifications for mounting approach lights in the United States are available in Ref. 10.

For operations in reduced visibility such as category II or lower, the International Civil Aviation Organization specifications are used for the lighting within 1000 ft of the runway threshold. The remaining 2000 ft of the lighting system is left as is. For the standard configuration-A system, this means that nine rows consisting of three red lights each are placed on either side of the centerline between the threshold bar and the cross bar. Additionally, two rows with four white lights each are placed at 500 ft from the threshold, symmetrically about the centerline. Detailed layout of the category II approach lighting system is described in Ref. 6.

A medium approach lighting system (MALS) is often used at smaller airports for nonprecision approaches. This system is only 1400 ft long as opposed to the 3000-ft-long standard configuration-A approach lighting system. Also, the threshold bar is not continuous. Only four lights are placed on each side of the threshold to indicate the approach direction. A MALS layout is also given in Ref. 6.

The runway lighting system consists of edge lights, centerline lights, and touchdown zone lights. A typical runway lighting layout is shown in Fig. 3. Standards for design and installation of runway lighting systems are given in Refs. 11 and 12.

The runway edge lights are high-intensity white lights, except for the last 2000 ft. In the last 2000 ft they are colored yellow to indicate a caution zone. The edge lights are located 10 ft away from the pavement, and the distance between the lights is 200 ft.

The centerline lights are 50 ft apart and run all the way to the end of the runway. The first centerline light is 75 ft from the runway threshold. These lights are white, except for the last 3000 ft in the approach direction where they are color coded. The lights for the first 2000 ft are alternately red and white, whereas the last 1000 ft are all red.

The touchdown zone lights start at 100 ft from the runway threshold and extend to 3000 ft in the direction of approach. The zone lights consist of three white lights, which are 5 ft apart and located at a distance of 30 ft about the centerline. The rows of zone lights are 100 ft apart from each other.

IV. Reference Frames

To utilize the visual information provided by the airport lighting for estimating the runway relative position and orientation of the aircraft, the lighting geometry has to be related to its image acquired by an onboard camera as a function of runway relative position and orientation of the aircraft. This requires several reference frames and an imaging model. These are described in this section.

Various reference frames used are illustrated in Fig. 4. In this figure, i is the origin of the inertial frame attached to the runway threshold. Because the locations of all lights are given with respect to the threshold bar, it is a natural choice for the location of the origin of the inertial reference frame. Furthermore, because the centerline lights form an axis of symmetry, following the flight dynamics convention, the x axis of the inertial frame is aligned with the runway centerline in the approach direction, and the z axis points down. The y axis completes the right-handed triad. The origin of the aircraft body axes is located at the point b, which is also the aircraft center of mass. Its position with respect to the inertial frame is given by the vector $\boldsymbol{X}_b^i$ with components x_b, y_b, and z_b in the inertial frame. The camera frame is located at c. The camera position with respect to the body frame is given by the vector $\boldsymbol{X}_c^b$ with components l_x, l_y, and l_z in the body frame. Because the camera is rigidly attached to the aircraft structure, the vector $\boldsymbol{X}_c^b$ is assumed to be constant in the present research. Let p be a light on the runway, and let its position with respect to the inertial frame be given by the vector $\boldsymbol{X}_p^i$ with components x_p, y_p, and z_p in the inertial frame. Also, let the position of point p with respect to the camera frame be given by the vector $\boldsymbol{X}_p^c$ with components x_{cp}, y_{cp}, and z_{cp} in the camera frame.

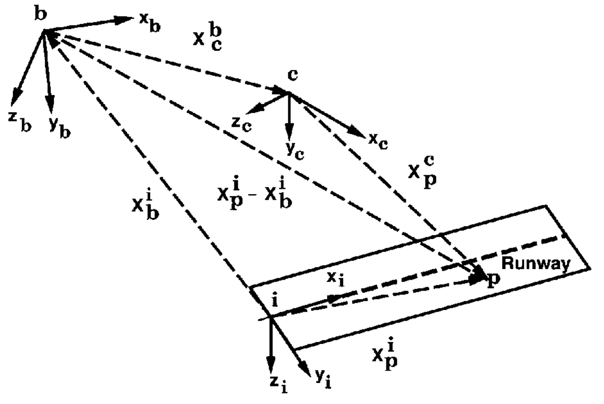

Fig. 4 Reference frames.

The position of the point p with respect to the aircraft with components in the inertial frame is given by the vector

$$\boldsymbol{X}_p^i - \boldsymbol{X}_b^i = [(x_p - x_b), (y_p - y_b), (z_p - z_b)]^T \tag{2}$$

The transformation matrix from the inertial frame to the body frame $\boldsymbol{T}_{b/i}$ can be obtained in terms of the yaw attitude ψ, pitch attitude θ, and roll attitude ϕ as[13]

$$\boldsymbol{T}_{b/i} = \begin{bmatrix} \cos\psi\cos\theta & \sin\psi\cos\theta & -\sin\theta \\ -\sin\psi\cos\phi + \cos\psi\sin\theta\sin\phi & \cos\psi\cos\phi + \sin\psi\sin\theta\sin\phi & \cos\theta\sin\phi \\ \sin\psi\sin\phi + \cos\psi\sin\theta\cos\phi & -\cos\psi\sin\phi + \sin\psi\sin\theta\cos\phi & \cos\theta\cos\phi \end{bmatrix} \tag{3}$$

The position of point p with respect to the aircraft with components along the body frame axes can be obtained as

$$\boldsymbol{X}_p^b = \boldsymbol{T}_{b/i}\left(\boldsymbol{X}_p^i - \boldsymbol{X}_b^i\right) \tag{4}$$

Similarly, the position of point p with respect to the camera frame resolved in Cartesian components along camera frame axes is given by

$$\boldsymbol{X}_p^c = \boldsymbol{T}_{c/b}\left(\boldsymbol{X}_p^b - \boldsymbol{X}_c^b\right) \tag{5}$$

where $\boldsymbol{T}_{c/b}$ is the constant transformation matrix from the body frame to the camera frame. Combining Eqs. (4) and (5),

$$\boldsymbol{X}_p^c = \boldsymbol{T}_{c/b}\boldsymbol{T}_{b/i}\left(\boldsymbol{X}_p^i - \boldsymbol{X}_b^i\right) - \boldsymbol{T}_{c/b}\boldsymbol{X}_c^b \tag{6}$$

Because the camera is assumed to be fixed with respect to the body, the product $-\boldsymbol{T}_{c/b}\boldsymbol{X}_c^b$ is a known constant vector $\boldsymbol{k}$ with components k_x, k_y, and k_z along the camera frame axes. Furthermore, if r_1–r_9 are defined as the elements of the transformation matrix from the inertial frame to the camera frame, $\boldsymbol{T}_{c/i} = \boldsymbol{T}_{c/b}\boldsymbol{T}_{b/i}$, the components of the position vector $\boldsymbol{X}_p^c$ can be obtained from Eq. (6) as

$$x_{cp} = r_1(x_p - x_b) + r_2(y_p - y_b) + r_3(z_p - z_b) + k_x \tag{7}$$

$$y_{cp} = r_4(x_p - x_b) + r_5(y_p - y_b) + r_6(z_p - z_b) + k_y \tag{8}$$

$$z_{cp} = r_7(x_p - x_b) + r_8(y_p - y_b) + r_9(z_p - z_b) + k_z \tag{9}$$

Equations (7–9) show the relationships between the location of the airport lights in the camera frame and the aircraft position and orientation.

The location of the light p in the image plane is given by the perspective projection equations based on the pinhole camera model shown in Fig. 5. The camera reference frame has its origin at c (Fig. 4). The x axis of the camera frame is aligned with the optic axis. The z axis points down, and the y axis completes the right-handed coordinate system. Based on the geometry shown in Fig. 5, the components of the position vector $\boldsymbol{X}_p^c$ can be related to the image coordinates u_p and v_p by the following two perspective projection equations[14]:

$$\frac{u_p - u_c}{f} = \frac{y_{cp}}{x_{cp}} \tag{10}$$

$$\frac{v_p - v_c}{f} = \frac{z_{cp}}{x_{cp}} \tag{11}$$

where u_c and v_c are coordinates of the camera center with respect to the image frame origin located at the top left-hand corner of the image and f is focal length of the camera. The u axis is directed from left to right, and the v axis is directed from top to bottom of the image plane. Introducing u_c and v_c coordinates results in positive u_p and v_p coordinates. Note that the images generated by real cameras produce discrete pixel locations indexed by rows and columns.

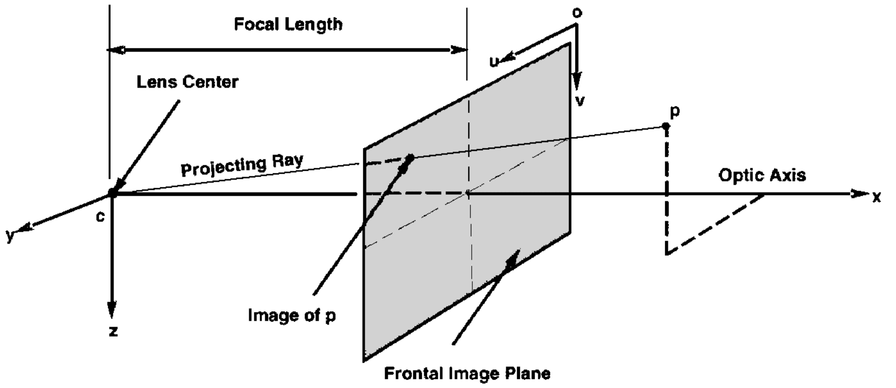

Fig. 5 Pinhole camera with frontal image plane.

V. Position and Attitude Estimation

Each airport light p within the field of view of the camera appears at (u_p, v_p) location in the image acquired by the camera. Equations (10) and (11) relate this location to the location in the camera frame. The camera relative location can be obtained in terms of the inertial location and orientation using Eqs. (7–9). Thus, if the locations of several lights in the image are associated with their respective inertial locations, Eqs. (7–11) can be used for determination of the runway relative position and orientation of the aircraft.

If the u_p and v_p location of two lights could be identified unambiguously and if the camera orientation is known, the position of the camera can be uniquely determined. This follows from the fact that Eqs. (7–9), when combined with Eqs. (10) and (11), result in two equations with three unknowns: x_b, y_b, and z_b. Because both the inertial location and the image plane location are known, x_p, y_p, z_p, u_p, and v_p are known. Two lights yield four such equations with three unknowns that can be solved to obtain a least-squares position estimate. If more than two lights can be identified, a more complex least-squares solution can be obtained.

Problem complexity increases considerably if, in addition to the runway relative position, the orientation is also unknown. Initially, it appears from Eqs. (7–11) that a complete solution requires determination of the three position components and nine elements r_1–r_9 of the transformation matrix. This, however, is not true. By using the orthogonality and right-handed property of the transformation matrix, it is known that the transformation matrix can be written as[15]

$$
\boldsymbol{T}_{c/i} = \begin{bmatrix} r_1 & r_2 & \pm\sqrt{1 - r_1^2 - r_2^2} \\ r_4 & r_5 & \pm\sqrt{1 - r_4^2 - r_5^2} \\ \pm\sqrt{1 - r_1^2 - r_4^2} & \pm\sqrt{1 - r_2^2 - r_5^2} & \pm\sqrt{-1 + r_1^2 + r_2^2 + r_4^2 + r_5^2} \end{bmatrix} \tag{12}
$$

It has been shown in Ref. 15 that, if r_1, r_2, r_4, and r_5 and the sign associated with r_3 can be found, the other elements can be determined. Hence, the complete solution requires determination of five quantities of the transformation matrix and three position components. As discussed earlier, each light that is successfully located both in the inertial and image frames provides two equations; thus, a minimum of four lights are needed for solution of the problem. Clearly these four lights should provide an independent set of equations. It may also be noted that Eqs. (7–9) are nonlinear in terms of the unknown quantities.

The methods discussed earlier require the image coordinates and the corresponding inertial coordinates of several lights. This correspondence is not easy because in black and white images there are no distinguishing features between lights. Additional information such as color and ordering of the lights is essential for successful correspondence. For the present study, black and white images are assumed. Instead of resorting to direct correspondence, the overall shape features of the lighting layout observed in the image can be used for establishing correspondence with shape features of the model to enable solution of the problem. This procedure is shown in Fig. 6. The solution procedure relies on the fact that an image of the lighting layout can be predicted using the camera model with assumed camera position and orientation. Thus, the difference of the features extracted from the predicted image and that extracted from the actual image of the airport lighting as seen by the camera can be recursively driven to zero to estimate the position and orientation of the aircraft with respect to the runway reference frame. It may be observed that the procedure described in Fig. 6 closely follows the traditional state estimation procedure used in control theory.

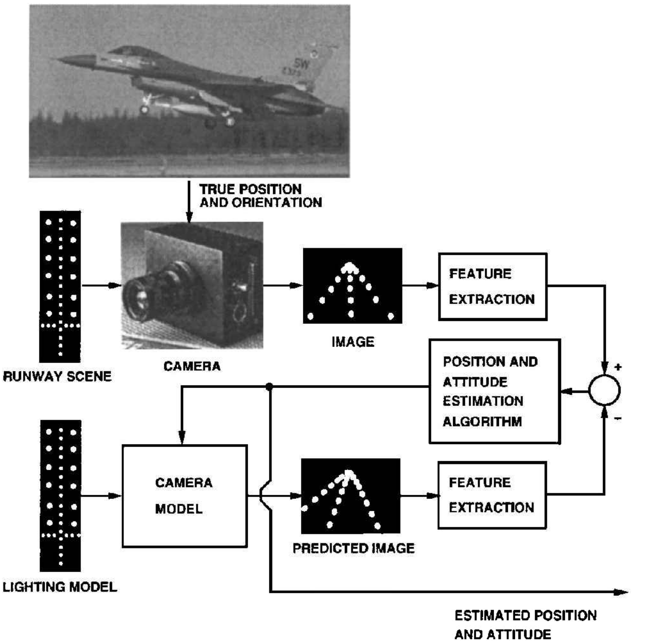

Fig. 6 Solution family using shape properties in the image plane.

The keys to state estimation using the procedure in Fig. 6 are the shape features. A few shape features based on statistical properties of the distribution of the airport lighting arrangement in the image plane are defined in the following. Raw measurement from the camera image consists of the coordinates of the lights observed in the image plane. Let the coordinates of light p be $(\tilde{u}_p, \tilde{v}_p)$ such that

$$\tilde{u}_p = u_p + \eta_u \tag{13}$$

$$\tilde{v}_p = v_p + \eta_v \tag{14}$$

with η_u and η_v representing the errors in the imaging process. The terms η_u and η_v are assumed to be independent scalar white noise processes. The coordinates of several lights can be combined for constructing shape features such as arithmetic means and higher-order moments. The following six image-based shape features employed in Ref. 5 are also used here:

$$z_1 = \sum_{1 \le p \le N} \frac{\tilde{u}_p}{N} \tag{15}$$

$$z_2 = \sum_{1 \le p \le N} \frac{\tilde{v}_p}{N} \tag{16}$$

$$z_3 = \sum_{1 \le p \le N} \frac{\left(\sqrt{\tilde{u}_p^2 + \tilde{v}_p^2}\right)}{N} \tag{17}$$

$$z_4 = \sqrt{\sum_{1 \le p \le N} \frac{(\tilde{v}_p - z_2)^2}{N}} \tag{18}$$

$$z_5 = \sqrt{\sum_{1 \le p \le N} \frac{(\tilde{u}_p - z_1 + \tilde{v}_p - z_2)^2}{2N}} \tag{19}$$

$$z_6 = \sqrt{\sum_{1 \le p \le N} \frac{(\tilde{u}_p - z_1)^2}{N}} \tag{20}$$

The term N in the preceding equations is the number of lights detected in the image. It may be verified that errors in these shape features are of the order of errors in the imaging process. The last three shape features given in Eqs. (18–20) may be compactly written as

$$z_j = \sqrt{\sum_{1 \le p \le N} \frac{[(\tilde{u}_p - z_1)\sin\tau_j + (\tilde{v}_p - z_2)\cos\tau_j]^2}{N}} \tag{21}$$

with $\tau_j = 0$, 45, and 90 deg for $j = 4$, 5, and 6, respectively.

The first and second shape features are the arithmetic means of positions of the lights visible in the image plane. The third shape feature is the mean distance from the origin of the image frame. The fourth shape feature is the moment about an axis that is parallel to the u axis and passes through the point defined by the mean. Similarly, the fifth shape feature is the moment about an axis that passes through the point defined by the mean and is inclined at 45 deg to both the u and v image axes. Finally, the sixth shape feature is the moment about an axis that passes through the mean and is parallel to the v axis.

The shape features described in Eqs. (15–20) can be related to the runway relative position and orientation states of the aircraft via the vector of functions $\boldsymbol{h}[\boldsymbol{X}(k)]$ at the kth time instant as

$$\boldsymbol{Z}(k) = \boldsymbol{h}[\boldsymbol{X}(k)] + \zeta_z(k) \tag{22}$$

where $\boldsymbol{Z}(k)$ is the 6×1 vector of shape features z_1–z_6, $\boldsymbol{X}(k)$ is the state vector, and $\zeta_z(k)$ is the 6×1 vector of white noise sequences with covariance $\boldsymbol{R}(k)$. The white noise sequences are assumed to model the errors in the shape features. Observe that the errors in shape features result from the errors in the raw measurements in Eqs. (13) and (14). From Fig. 6 it may be seen that, if an accurate estimate of the runway relative position and the orientation of the aircraft were available, the differences between the shape features computed from the actual image and the predicted image would be due to errors in the imaging process. The elements h_1–h_6 of the vector of functions $\boldsymbol{h}[\boldsymbol{X}(k)]$ are also given by the shape features listed in Eqs. (15–20) except that the values are computed using the image coordinates u_p and v_p of the lights in the predicted image instead of $\tilde{u}_p$ and $\tilde{v}_p$, which are based on the actual image. Note that, for these computations, the number of lights observed in the predicted image M has to be used instead of N, which is the number of lights observed in the actual image. Initially, the number of lights in the predicted images and that in the actual images are quite different because of the differences between the estimated and the actual states of the aircraft. As the estimates improve, the number of lights in the predicted image approaches the number of lights observed in the actual image.

In addition to the relationship between the scalar features and the runway relative position and orientation states of the aircraft at every time instant, the temporal evolution of states are given by the equations of motion of the aircraft. The six-degree-of-freedom equations of motion are described in Ref. 13. Using only the kinematic equations, the temporal evolution of the states can be described by a linear discrete time state model of the form

$$\boldsymbol{X}(k+1) = \boldsymbol{\Phi}(k)\boldsymbol{X}(k) + \zeta_x(k) \tag{23}$$

where $\boldsymbol{X}(k)$ is the state vector at the kth time epoch. To represent a six-degree-of-freedom model of the aircraft, 12 states are adequate. Because the roll attitude angle is assumed to be available from a roll sensor, the two states consisting of the roll attitude angle and the roll rate are not needed. The state model can therefore be constructed by using the following 10 states: 3 components of the runway relative aircraft position x_b, y_b, and z_b; 3 components of the aircraft inertial velocity V_{bx}, V_{by}, and V_{bz}; yaw and pitch Euler angles ψ and θ; and the yaw and pitch body rates r and q. With these 10 states, the state transition matrix

$$\boldsymbol{\Phi}(k) = \begin{bmatrix} 1 & 0 & 0 & \Delta t & 0 & 0 & 0 & 0 & 0 & 0 \\ 0 & 1 & 0 & 0 & \Delta t & 0 & 0 & 0 & 0 & 0 \\ 0 & 0 & 1 & 0 & 0 & \Delta t & 0 & 0 & 0 & 0 \\ 0 & 0 & 0 & 1 & 0 & 0 & 0 & 0 & 0 & 0 \\ 0 & 0 & 0 & 0 & 1 & 0 & 0 & 0 & 0 & 0 \\ 0 & 0 & 0 & 0 & 0 & 1 & 0 & 0 & 0 & 0 \\ 0 & 0 & 0 & 0 & 0 & 0 & 1 & 0 & \cos\phi(k)\sec\theta(k)\Delta t & \sin\phi(k)\sec\theta(k)\Delta t \\ 0 & 0 & 0 & 0 & 0 & 0 & 0 & 1 & -\sin\phi(k)\Delta t & \cos\phi(k)\Delta t \\ 0 & 0 & 0 & 0 & 0 & 0 & 0 & 0 & 1 & 0 \\ 0 & 0 & 0 & 0 & 0 & 0 & 0 & 0 & 0 & 1 \end{bmatrix} \tag{24}$$

can be formed by assuming that the orientation angles are constant during the time interval Δt. During landing, the aircraft trajectory is expected to closely follow the glide slope. Minor deviations about this nominal trajectory can be modeled by driving the linear and angular acceleration components by white noise. This is accomplished via $\zeta_x(k)$, which is a vector of discrete time white noise sequences with covariance $\boldsymbol{Q}(k)$.

Given the fact that a measurement equation of the form in Eq. (22) and a state equation of the form in Eq. (23) can be formed, the runway relative position and orientation estimation problem can be conveniently cast as a Kalman filtering problem. Using the measurement and state equations, the state estimate and its error covariance can be computed recursively using the Kalman filter.[16] Because the steps required for implementing Kalman filters are well known and available in several textbooks, only a brief description of the Kalman filter algorithm is provided in the Appendix. The details of the various matrices that are required for implementing the Kalman filter are also described in the Appendix.

VI. Simulation and Results

The performance of the position estimation algorithm described in Fig. 6 is evaluated using a computer simulation.

To simulate the imaging process, the camera is assumed to be fixed to the aircraft, looking down along a 3-deg glide slope. The camera focal length is assumed to be 600 pixels, and the image is assumed to be digitized on a 512×512 pixel array. For image synthesis, the true location and orientation of the aircraft and the known inertial location of the lights are used in Eqs. (7–9). The resulting coordinates with respect to the camera frame are used in the perspective projection equations, Eqs. (10) and (11), to compute the u_p and v_p image locations. These locations are then quantized within 1 pixel by using a quantization interval of half a pixel and are marked in the image plane. The image is then clipped to fit within the camera's field of view. A sample simulated image is shown in Fig. 7. This image corresponds to the camera located at an altitude of 95 and 812 ft downrange from runway threshold.

For generating measurements for the Kalman filter, the image coordinates $\tilde{u}_p$ and $\tilde{v}_p$ corresponding to visible lights are first extracted from the simulated image. Next, the image coordinates $\tilde{u}_p$ and $\tilde{v}_p$ are used in Eqs. (15–20) for computing the measurements z_1–z_6. It may be noted that the lights that are farther from the camera are merged together in the image plane due to perspective projection as shown in Fig. 7. Thus, fewer than the actual number of lights are detectable and available for processing.

Like the elements of the measurement vector $\boldsymbol{Z}(k)$, the elements of the measurement model vector $\boldsymbol{h}[\boldsymbol{X}(k)]$ are also computed using Eqs. (15–20) for the Kalman filter. However, in this case, the image coordinates are based on the predicted image as shown in Fig. 6. The predicted image is constructed using the airport lighting database, the estimated position, and yaw and pitch orientations of the aircraft along with the known roll orientation. Note that this image is different from that acquired by the camera. To make the predicted measurements compatible with the actual measurements, light positions in the database that appear within 1 pixel in the image plane are counted only once.

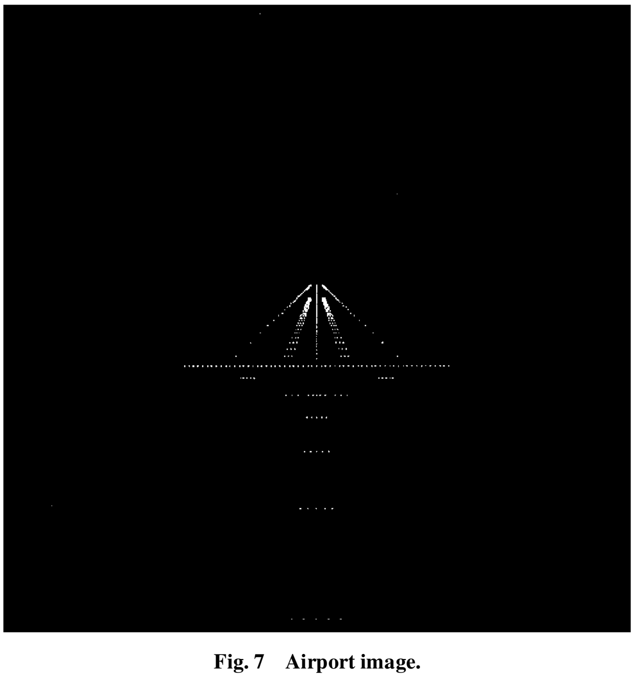

Fig. 7 Airport image.

In addition to the measurement model vector that is based on the predicted image, the observation matrix needed by the Kalman filter is also computed using the predicted image, estimated state, and the known roll orientation.

To evaluate the performance of the proposed position estimation system, the aircraft flight along the glide slope shown in Fig. 1 was simulated. At the beginning of the simulation, the aircraft is at 400 ft altitude and 6633 ft downrange from the runway threshold. Its approach speed is 220 ft/s. The aircraft is crabbed at a 10-deg angle with respect to the runway centerline to compensate for crosswind. Thus, the crossrange is zero throughout the approach and landing phases. The total duration of the flight beginning at 400 ft altitude and ending at the touchdown point is 34 s.

For the landing scenario simulated, initially both the approach lights and the runway lights are visible in the image. As the aircraft proceeds along the descent path, the approach lights start moving out of the field of view below 230 ft altitude. Finally, below 70 ft altitude, the threshold bar and other runway lights move out of the field of view of the camera. Fortunately, this does not cause problems for the algorithm because by then the state estimates are converged; therefore, lights not seen in the actual image are also not seen in the predicted image.

For generating numerical results using the vision-based algorithm described in this paper, the Kalman filter was initialized with the runway relative position components in error by 1000 ft along the x axis, 100 ft along the y axis, and 100 ft along the z axis with respect to their true values. The inertial velocity states, orientation states, and the body rate states were all set to zero.

The error residuals for the position components for the chosen initial conditions are shown in Fig. 8. The error residual is defined as the difference between the estimated and the actual values. It may be observed that it takes about 5 s for the along-track estimate to converge to within ± 100 ft. The cross-track position and altitude estimates, which are more critical for landing, converge to within ± 5 ft in 1 s and ± 12 ft in 6 s, respectively. The cross-track position and altitude error residuals at several decision heights (DH) are summarized in Table 2.

The error residuals for the yaw and pitch orientations are given in Fig. 9. It may be seen that the estimates converge to within ± 0.2 deg in less than 1 s. Starting with initial errors in the yaw and pitch orientations of 10 and 3 deg, the algorithm is able to correctly estimate these angles. Note that the initial errors in the yaw and pitch orientation angles are significant. An error of 10 deg in the yaw orientation angle translates into a 22-kn crosswind correction based on the approach speed of 130 kn. A crosswind of 22 kn is considered to be large for a general aviation aircraft.[6] The 3-deg pitch orientation angle error assumes that the camera is looking straight ahead while the actual camera is aligned along the glide slope.

The usefulness of the estimation scheme can be assessed by comparing the achieved accuracy with the desired accuracies listed in Table 1. It may be seen from Table 2 that the present navigation scheme meets the CAT I objectives listed in Table 1. Additionally, it meets the cross-track accuracy requirements for CAT II and CAT III. The algorithm is also able to provide very accurate yaw and pitch attitude estimates. Because the yaw orientation angle and the pitch orientation angle of the camera are related to the aircraft crab angle and the glide slope, the algorithm can be used for providing this important information.

The attempts to extend this algorithm for roll orientation angle estimation were unsuccessful using the available measurements. In addition to the six measurements, the correlation coefficient in Ref. 14, orientation of the principal axis in Ref. 17, and the eigenvalues of the covariance matrix were used as additional measurements. A possible reason for the inability to estimate the roll angle based on these

Table 2 Position error residuals

Category	DH, ft	Cross track, ft	Altitude, ft
I	$200 \le h \le 300$	± 0.60	± 11.29
II	$100 \le h < 200$	± 0.25	± 10.10
IIIa	$50 \le h < 100$	± 0.85	± 2.54
IIIb and c	$10 \le h < 50$	± 1.36	± 0.86

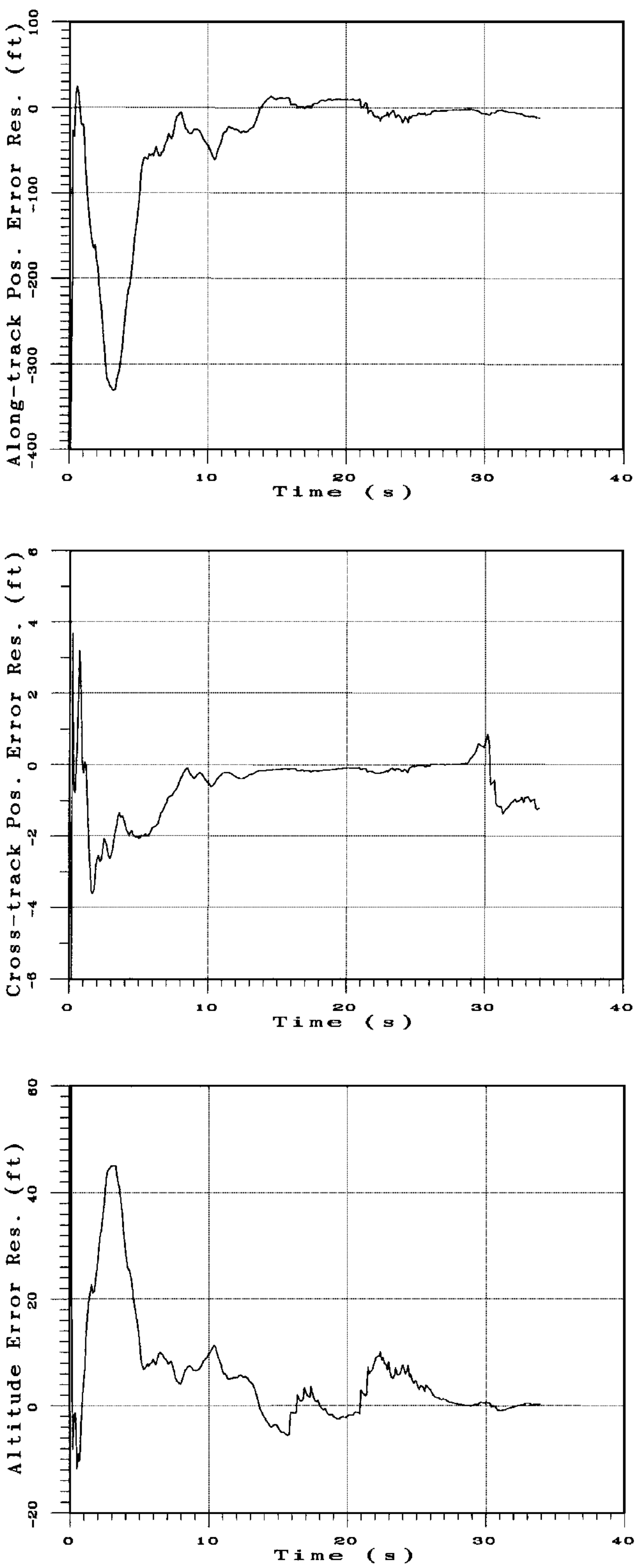

Fig. 8 Error in position estimates.

measurements is that no additional information useful for roll angle estimation is contained in these measurements. The complete information from the covariance matrix is already captured by the z_4–z_6 measurements. It is therefore recommended that roll estimation should be attempted by considering measures based on higher-order moments. However, it should be noted that higher-order moments in general have increasingly smaller magnitudes.[17] This fact may have a significant impact for roll orientation angle estimation because a Kalman filter, like other least-squares estimators, is biased toward larger errors. The errors associated with smaller magnitude measurements may be smaller.

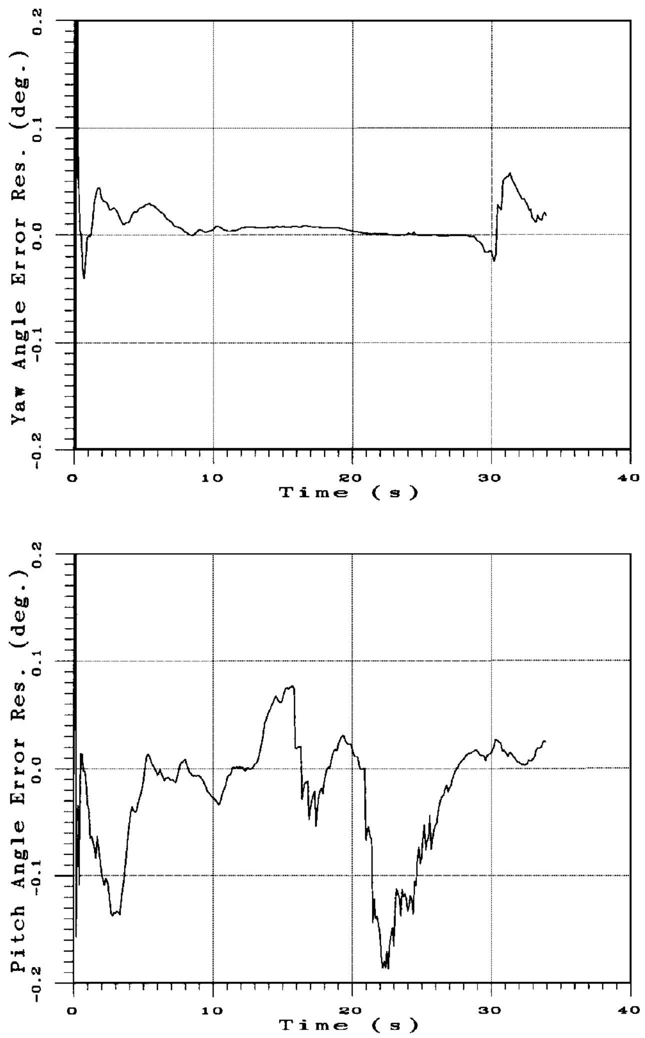

Fig. 9 Error in yaw and pitch orientation estimates.

VII. Conclusions

A vision-based algorithm for estimation of runway relative position components and yaw and pitch attitudes during night approach and landing was described. The algorithm uses a Kalman filter to integrate airport images acquired by an onboard camera, a model of the airport lighting, a kinematic model of the aircraft, and the measured roll orientation. In addition to the position and attitude estimates, the Kalman filter provides estimates of the inertial velocity and yaw and pitch angular rates. The performance of the estimation algorithm was evaluated in a computer simulation. The cross-track position and altitude estimation errors resulting from the algorithm were found to be well within category I performance objectives. Lateral accuracy for categories II and III was also met. Additionally, the algorithm was able to provide accurate estimates of the yaw and pitch orientation angles.

Appendix: Kalman Filter Algorithm

Present formulation of the Kalman filter follows the research reported in Ref. 18. To set up the Kalman filter, the measurement equation given in Eq. (22) and the state equation given in Eq. (23) are used. The Kalman filter consists of two parts, namely, measurement update and process update. The measurement part of the Kalman filter improves the estimate of state and its covariance based on a new measurement. The updated values are

$$\tilde{\boldsymbol{X}}(k) = \hat{\boldsymbol{X}}(k) + \boldsymbol{K}(k)\{\boldsymbol{Z}(k) - \boldsymbol{h}[\hat{\boldsymbol{X}}(k)]\} \tag{A1}$$

$$\tilde{\boldsymbol{P}}(k) = [\boldsymbol{I} - \boldsymbol{K}(k)\boldsymbol{H}(k)]\boldsymbol{P}(k) \tag{A2}$$

where $\hat{\boldsymbol{X}}(k)$ is the estimated state vector, $\boldsymbol{Z}(k)$ is the measurement vector based on the camera image, $\boldsymbol{h}[\hat{\boldsymbol{X}}(k)]$ is the measurement model vector based on the predicted image, $\boldsymbol{K}(k)$ is the Kalman gain matrix, $\boldsymbol{I}$ is the identity matrix, $\boldsymbol{H}(k)$ is the observation matrix, and $\boldsymbol{P}(k)$ is the state error covariance matrix. The Kalman gain is computed using

$$\boldsymbol{K}(k) = \boldsymbol{P}(k)\boldsymbol{H}^T(k)[\boldsymbol{H}(k)\boldsymbol{P}(k)\boldsymbol{H}^T(k) + \boldsymbol{R}(k)]^{-1} \tag{A3}$$

where $\boldsymbol{R}(k)$ is the measurement noise covariance matrix. The observation matrix $\boldsymbol{H}(k)$ is evaluated as follows:

$$\boldsymbol{H}(k) = \left.\frac{\partial \boldsymbol{h}(\boldsymbol{X})}{\partial \boldsymbol{X}}\right|_{X=\hat{X}(k)} \tag{A4}$$

The time update or process update part of the Kalman filter accounts for system dynamics and propagates the state and its error covariance until the next measurement is taken. The propagated values are

$$\hat{\boldsymbol{X}}(k+1) = \Phi(k)\tilde{\boldsymbol{X}}(k) \tag{A5}$$

$$\boldsymbol{P}(k+1) = \Phi(k)\tilde{\boldsymbol{P}}(k)\Phi^T(k) + \boldsymbol{Q}(k) \tag{A6}$$

where $\Phi(k)$ is the state transition matrix given in Eq. (24) and $\boldsymbol{Q}(k)$ is the process noise covariance matrix. The other quantities are as defined before.

The key element of successful implementation of the Kalman filter is the construction of the observation matrix $\boldsymbol{H}(k)$. Computation of the $\boldsymbol{H}(k)$ matrix requires partial derivatives of the elements of the $\boldsymbol{h}(\boldsymbol{X})$ vector with respect to the estimated state. Because the elements of the $\boldsymbol{h}(\boldsymbol{X})$ vector, h_1–h_6, are related to the aircraft position and orientation states via the image coordinates u_p and v_p, the partial derivatives of u_p and v_p are required as intermediate steps. These partial derivatives can be evaluated from Eqs. (10) and (11) as follows:

$$\frac{\partial u_p}{\partial \delta_i} = f\frac{x_{cp}(\partial y_{cp}/\partial \delta_i) - y_{cp}(\partial x_{cp}/\partial \delta_i)}{x_{cp}^2} \tag{A7}$$

$$\frac{\partial v_p}{\partial \delta_i} = f\frac{x_{cp}(\partial z_{cp}/\partial \delta_i) - z_{cp}(\partial x_{cp}/\partial \delta_i)}{x_{cp}^2} \tag{A8}$$

where $i = 1, \ldots, 5$ and $\delta_1, \ldots, \delta_5$ correspond to the aircraft position and orientation states: x_b, y_b, z_b, ψ, and θ. The term f is the focal length of the camera. The partial derivatives of x_{cp}, y_{cp}, and z_{cp} can be obtained from Eqs. (7–9) as

$$\frac{\partial x_{cp}}{\partial \delta_1} = -r_1 \tag{A9}$$

$$\frac{\partial x_{cp}}{\partial \delta_2} = -r_2 \tag{A10}$$

$$\frac{\partial x_{cp}}{\partial \delta_3} = -r_3 \tag{A11}$$

$$\frac{\partial x_{cp}}{\partial \delta_4} = (x_p - x_b)\frac{\partial r_1}{\partial \delta_4} + (y_p - y_b)\frac{\partial r_2}{\partial \delta_4} + (z_p - z_b)\frac{\partial r_3}{\partial \delta_4} \tag{A12}$$

$$\frac{\partial x_{cp}}{\partial \delta_5} = (x_p - x_b)\frac{\partial r_1}{\partial \delta_5} + (y_p - y_b)\frac{\partial r_2}{\partial \delta_5} + (z_p - z_b)\frac{\partial r_3}{\partial \delta_5} \tag{A13}$$

$$\frac{\partial y_{cp}}{\partial \delta_1} = -r_4 \tag{A14}$$

$$\frac{\partial y_{cp}}{\partial \delta_2} = -r_5 \tag{A15}$$

$$\frac{\partial y_{cp}}{\partial \delta_3} = -r_6 \tag{A16}$$

$$\frac{\partial y_{cp}}{\partial \delta_4} = (x_p - x_b)\frac{\partial r_4}{\partial \delta_4} + (y_p - y_b)\frac{\partial r_5}{\partial \delta_4} + (z_p - z_b)\frac{\partial r_6}{\partial \delta_4} \tag{A17}$$

$$\frac{\partial y_{cp}}{\partial \delta_5} = (x_p - x_b)\frac{\partial r_4}{\partial \delta_5} + (y_p - y_b)\frac{\partial r_5}{\partial \delta_5} + (z_p - z_b)\frac{\partial r_6}{\partial \delta_5} \tag{A18}$$

$$\frac{\partial z_{cp}}{\partial \delta_1} = -r_7 \tag{A19}$$

$$\frac{\partial z_{cp}}{\partial \delta_2} = -r_8 \tag{A20}$$

$$\frac{\partial z_{cp}}{\partial \delta_3} = -r_9 \tag{A21}$$

$$\frac{\partial z_{cp}}{\partial \delta_4} = (x_p - x_b)\frac{\partial r_7}{\partial \delta_4} + (y_p - y_b)\frac{\partial r_8}{\partial \delta_4} + (z_p - z_b)\frac{\partial r_9}{\partial \delta_4} \tag{A22}$$

$$\frac{\partial z_{cp}}{\partial \delta_5} = (x_p - x_b)\frac{\partial r_7}{\partial \delta_5} + (y_p - y_b)\frac{\partial r_8}{\partial \delta_5} + (z_p - z_b)\frac{\partial r_9}{\partial \delta_5} \tag{A23}$$

where r_1–r_9 are the components of the inertial frame to camera frame transformation matrix similar to those in Eq. (3).

Once these partial derivatives are evaluated for each light p in the image plane, partial derivatives of h_1, h_2, and h_3 are computed as follows:

$$\frac{\partial h_1}{\partial \delta_i} = \frac{1}{M}\sum_{1\le p\le M}\frac{\partial u_p}{\partial \delta_i} \tag{A24}$$

$$\frac{\partial h_2}{\partial \delta_i} = \frac{1}{M}\sum_{1\le p\le M}\frac{\partial v_p}{\partial \delta_i} \tag{A25}$$

$$\frac{\partial h_3}{\partial \delta_i} = \frac{1}{M}\sum_{1\le p\le M}\frac{u_p(\partial u_p/\partial \delta_i) + v_p(\partial v_p/\partial \delta_i)}{\sqrt{u_p^2 + v_p^2}} \tag{A26}$$

where M is the number of lights in the predicted image. Similarly, the partial derivatives of h_4, h_5, and h_6 are evaluated as

$$\frac{\partial h_j}{\partial \delta_i} = \frac{\Omega_{p,i,j}}{\sqrt{M\sum_{1\le p\le M}[(u_p - h_1)\sin\tau_j + (v_p - h_2)\cos\tau_j]^2}} \tag{A27}$$

with $\tau_j = 0$, 45, and 90 deg for $j = 4$, 5, and 6, respectively. The term $\Omega_{p,i,j}$ is given as

$$\Omega_{p,i,j} = \sum_{1\le p\le M}\Bigg\{[(u_p - h_1)\sin\tau_j + (v_p - h_2)\cos\tau_j] \times \left[\left(\frac{\partial u_p}{\partial \delta_i} - \frac{\partial h_1}{\partial \delta_i}\right)\sin\tau_j + \left(\frac{\partial v_p}{\partial \delta_i} - \frac{\partial h_2}{\partial \delta_i}\right)\cos\tau_j\right]\Bigg\} \tag{A28}$$

The complete observation matrix $\boldsymbol{H}(k)$ can now be written in terms of the partial derivatives of the six measurements:

$$\boldsymbol{H}(k) = \begin{bmatrix} \frac{\partial h_1}{\partial \delta_1} & \frac{\partial h_1}{\partial \delta_2} & \frac{\partial h_1}{\partial \delta_3} & 0 & 0 & 0 & \frac{\partial h_1}{\partial \delta_4} & \frac{\partial h_1}{\partial \delta_5} & 0 & 0 \\ \frac{\partial h_2}{\partial \delta_1} & \frac{\partial h_2}{\partial \delta_2} & \frac{\partial h_2}{\partial \delta_3} & 0 & 0 & 0 & \frac{\partial h_2}{\partial \delta_4} & \frac{\partial h_2}{\partial \delta_5} & 0 & 0 \\ \frac{\partial h_3}{\partial \delta_1} & \frac{\partial h_3}{\partial \delta_2} & \frac{\partial h_3}{\partial \delta_3} & 0 & 0 & 0 & \frac{\partial h_3}{\partial \delta_4} & \frac{\partial h_3}{\partial \delta_5} & 0 & 0 \\ \frac{\partial h_4}{\partial \delta_1} & \frac{\partial h_4}{\partial \delta_2} & \frac{\partial h_4}{\partial \delta_3} & 0 & 0 & 0 & \frac{\partial h_4}{\partial \delta_4} & \frac{\partial h_4}{\partial \delta_5} & 0 & 0 \\ \frac{\partial h_5}{\partial \delta_1} & \frac{\partial h_5}{\partial \delta_2} & \frac{\partial h_5}{\partial \delta_3} & 0 & 0 & 0 & \frac{\partial h_5}{\partial \delta_4} & \frac{\partial h_5}{\partial \delta_5} & 0 & 0 \\ \frac{\partial h_6}{\partial \delta_1} & \frac{\partial h_6}{\partial \delta_2} & \frac{\partial h_6}{\partial \delta_3} & 0 & 0 & 0 & \frac{\partial h_6}{\partial \delta_4} & \frac{\partial h_6}{\partial \delta_5} & 0 & 0 \end{bmatrix} \tag{A29}$$

In addition to the specification of the observation matrix, the process noise covariance matrix $\boldsymbol{Q}(k)$ and the measurement noise covariance matrix $\boldsymbol{R}(k)$ have to be specified for using the Kalman filter algorithm. Because six image-based measurements are used, the dimension of the measurement noise covariance matrix $\boldsymbol{R}(k)$ is

6×6. The variances of the errors due to the imaging process are assigned as diagonal elements of this matrix. The standard deviation of the measurement errors is assumed to be 0.5 pixels. Because 10 states are estimated, the process noise covariance matrix $\boldsymbol{Q}(k)$ is chosen to be a 10×10 diagonal matrix. The diagonal element values are selected to suitably tune the Kalman filter.

For initializing the filter, initial estimates of the state $\hat{\boldsymbol{X}}(0)$ and its error covariance matrix $\boldsymbol{P}(0)$ are required. Initially, large values are placed in the diagonal locations of the state error covariance matrix. The off-diagonal terms are set to zero. Large variance values result in a higher reliance on the measurement during the first few steps. As the state error covariance matrix converges, the Kalman filter weight on the process model increases.

Because the moment of inertia about the roll axis is the smallest, roll dynamics are the fastest. Assuming a roll time constant of 1 s for a general aviation aircraft[19] results in a Nyquist sample rate of two samples per second. Therefore, the integration time step should be chosen to be less than 0.5 s. The Kalman filter step size of 0.1 s is chosen in this research to be compatible with the camera frame rate of 10 frames per second.

References

[1] Baker, S. P., Lamb, M. W., Li, G., and Dodd, R. S., "Human Factors in Crashes of Commuter Airplanes," *Aviation, Space, and Environmental Medicine*, Jan. 1993, pp. 63–68.

[2] Bennett, C. T., and Schwirzke, M., "Analysis of Accidents During Instrument Approaches," *Aviation, Space, and Environmental Medicine*, April 1992, pp. 253–261.

[3] Haines, R. F., and Flatau, C., *Night Flying*, McGraw–Hill, Blue Ridge Summit, PA, 1992.

[4] McNally, B. D., Warner, D. N., Hegarty, D. M., Schultz, T. A., and Bronson, R., "Flight Evaluation of Precision Code Differential GPS for Terminal Area Positioning," *Proceedings of the 4th International Meeting of the Satellite Division of the Institute of Navigation (ION GPS-91)*, Inst. of Navigation, 1991, pp. 557–570.

[5] Chatterji, G. B., Menon, P. K., and Sridhar, B., "Integrated GPS/Machine-Vision Navigation System for Aircraft Night Operations," *Proceedings of AIAA Guidance, Navigation, and Control Conference*, AIAA, Washington, DC, 1995, pp. 214–224.

[6] Horonjeff, R., and McKelvey, F. X., *Planning and Design of Airports*, 3rd ed., McGraw–Hill, New York, 1983, pp. 503–534.

[7] Nolan, M. S., *Fundamentals of Air Traffic Control*, Wadsworth, Belmont, CA, 1994, pp. 92–94.

[8] "Flying Training: Instrument Flying," Dept. of the Air Force, AFM 51-37, Headquarters U.S. Air Force, Washington, DC, July 1986.

[9] "1994 Federal Radionavigation Plan," U.S. Dept. of Transportation and U.S. Dept. of Defense, DOT-VNTSC-RSPA-95-1/DOD-4650.5, National Technical Information Service, Springfield, VA, May 1995, pp. 2–14.

[10] "Airport Design Standards-Site Requirements for Terminal Navigational Facilities," Federal Aviation Administration, Advisory Circular AC 150/5300-2D, Washington, DC, March 1980.

[11] "Runway and Taxiway Edge Lighting System," Federal Aviation Administration, Advisory Circular AC 150/5340-24, Washington, DC, Nov. 1977.

[12] "Installation Details for Runway Centerline and Touchdown Zone Lighting Systems," Federal Aviation Administration, Advisory Circular AC 150/5340-4C, Washington, DC, Aug. 1978.

[13] Stevens, B. L., and Lewis, F. L., *Aircraft Control and Simulation*, Wiley, New York, 1992, p. 37.

[14] Duda, R. O., and Hart, P. E., *Pattern Classification and Scene Analysis*, Wiley, New York, 1973, pp. 247 and 379–382.

[15] Tsai, R. Y., "A Versatile Camera Calibration Technique for High-Accuracy 3D Machine Vision Metrology Using Off-the-Shelf TV Cameras and Lenses," *IEEE Journal of Robotics and Automation*, Vol. RA-3, No. 4, 1987, pp. 323–344.

[16] Anderson, B. D. O., and Moore, J. B., *Optimal Filtering*, Prentice–Hall, Englewood Cliffs, NJ, 1979, pp. 36–61.

[17] Jain, A. K., *Fundamentals of Digital Image Processing*, Prentice–Hall, Englewood Cliffs, NJ, 1989, pp. 377, 378, 392, 393.

[18] Sridhar, B., and Phatak, A. V., "Simulation and Analysis of Image-Based Navigation System for Rotorcraft Low Altitude Flight," *IEEE Transactions on Systems, Man, and Cybernetics*, Vol. 22, No. 2, 1992, pp. 290–299.

[19] Nelson, R. C., *Flight Stability and Automatic Control*, McGraw–Hill, New York, 1989, pp. 138–171.